Molecular Simulation of Carbon Dioxide/Methane/Hydrogen Mixture Adsorption in Metal−Organic Frameworks

Qingyuan Yang and Chongli Zhong*

Department of Chemical Engineering, Key Laboratory of Bioprocess of Beijing, Beijing University of Chemical Technology, Beijing 100029, China

Received: May 3, 2006; In Final Form: July 7, 2006

This work performs a systematic computational study toward a molecular understanding of the separation characteristics of metal−organic frameworks (MOFs), for which the purification of synthetic gas by two representative MOFs, MOF-5 and Cu-BTC, is adopted as an example. The simulations show that both geometry and pore size affect largely the separation efficiency, complex selectivity behaviors with different steps can occur in MOFs, and the electrostatic interactions that exist can enhance greatly the separation efficiency of gas mixtures composed of components with different chemistries. Furthermore, the macroscopic separation behaviors of the MOF materials are elucidated at a molecular level to give insight into the underlying mechanisms. The findings as well as the molecular-level elucidations provide useful microscopic information toward a complete understanding of the separation characteristics of MOFs that may lead to general design strategies for synthesizing new MOFs with tailored properties, as well as guiding their practical applications.

1. Introduction

Metal−organic frameworks (MOFs) have been recognized as an important family of nanoporous materials for their adjustable chemical functionality and fine-tunable pore structures.[1] Although they have shown great potential applications to separation and purification of gas mixtures by adsorption, to date most studies focused on the adsorption behavior of simple gases in them, both experimentally[2] and theoretically;[3] the investigations on the direct separation of gas mixtures by MOFs are very scarce.[4,5] Therefore, little is known on the separation characteristics of MOFs as well as if they have any special properties relative to more well-known materials.[6] On the other hand, the available investigations on MOFs have shown that one of the most promising practical applications of this kind of materials at the moment is for adsorption separation of gas mixtures, and thus the relevant knowledge is highly necessary and important both scientifically and practically.

In this work, a computational study was performed toward an understanding of the separation characteristics of MOFs. For this purpose, the purification of synthetic gas obtained from steam re-forming of natural gas was selected as an example. This is a very important practical system, since 95% of hydrogen used in fuel cells is now produced by this method, and components such as methane and carbon dioxide must be removed from the synthetic gas before hydrogen can be used effectively.[7] Although a variety of investigations have been performed for separation of this system in zeolites and other porous materials,[8] the studies on MOFs have not been performed, and in this work we adopted two typical MOFs with different topologies, the MOF-5 with a simple cubic framework[9] and the Cu-BTC with a channel/pocket complex framework,[10] as representatives of MOFs. The knowledge obtained is expected to apply to a broad range of MOFs for separation of various gas mixture systems of practical importance.

* Corresponding author. E-mail: zhongcl@mail.buct.edu.cn.

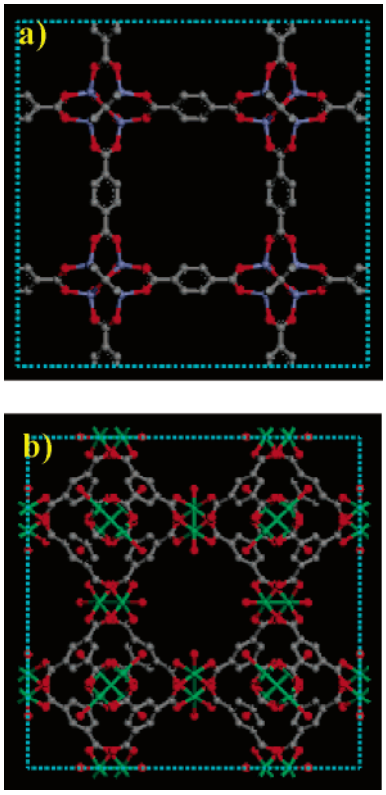

Figure 1. Unit cell crystal structures of the two MOFs viewed along the [100] direction: (a) MOF-5; (b) Cu-BTC (Zn, blue; Cu, green; O, red; C, gray, and H atoms are omitted for clarity).

2. Models and Simulation Method

2.1. MOF Structures. The crystal structures of MOF-5 and Cu-BTC were constructed from the X-ray diffraction (XRD) data[9,10] using Materials Visualizer,[11] and the unit cells are shown in Figure 1. As shown in Figure 1a, the crystal structure of MOF-5 is very simple, consisting of Zn_4O clusters connected

10.1021/jp062723w CCC: $33.50
Published on Web 08/19/2006

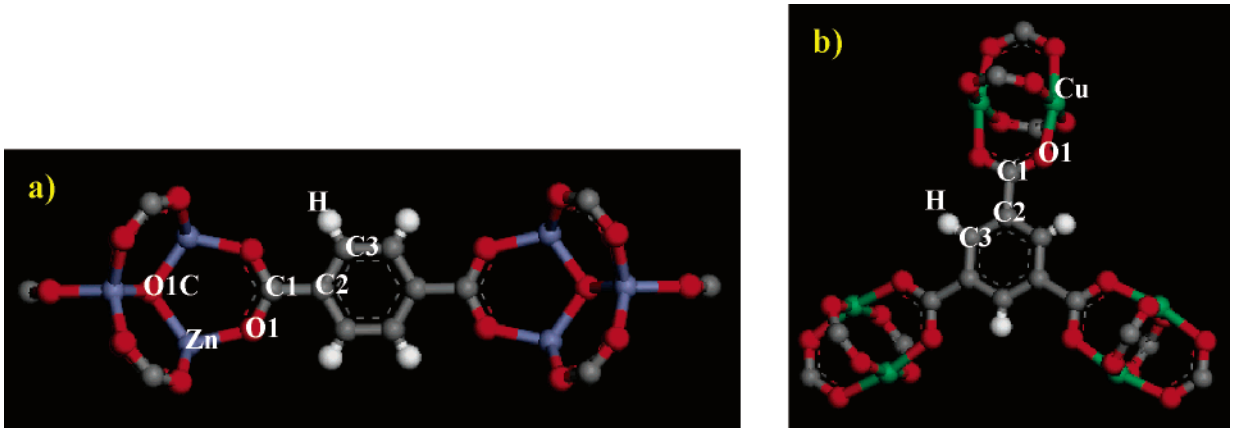

Figure 2. Model clusters used for the calculations of atomic partial charges: (a) MOF-5; (b) Cu-BTC.

by 1,4-benzenedicarboxylate (BDC) linkers to form a three-dimensional porous cubic framework with cavity diameter of ca. 1.4 nm. Cu-BTC (Figure 1b), on the other hand, is composed of $Cu_2(COO)_4$ paddle wheels with copper dimmers as four connectors and benzene-1,3,5-tricarboxylate (BTC) as three connectors, forming a three-dimensional network with main channels of a square cross-section of ca. 0.9 nm diameter and tetrahedral side pockets of ca. 0.5 nm, which are connected to the main channels by triangular windows of ca. 0.35 nm diameter. Obviously, the structure of MOF-5 is much simpler than Cu-BTC, and it has cubic pores with Zn_4O clusters in the corners, while the latter has two kinds of pores with smaller sizes. It should be pointed out that the crystal structure of Cu-BTC[10] includes axial oxygen atoms weakly bonded to the Cu atoms, which correspond to water ligands. The following study is performed on the dry Cu-BTC with these oxygen atoms removed.

2.2. Force Fields. In the present work, a single Lennard-Jones (LJ) interaction site model was used to describe a methane molecule, and the potential parameters ($\sigma_{CH_4} = 0.373$ nm and $\epsilon_{CH_4}/k_B = 148.0$ K) were taken from the TraPPE force field.[12] Carbon dioxide was modeled as a rigid linear triatomic molecule with three charged LJ interaction sites, for which the LJ potential parameters for atom O ($\sigma_O = 0.305$ nm and $\epsilon_O/k_B = 79.0$ K) and atom C ($\sigma_C = 0.280$ nm and $\epsilon_C/k_B = 27.0$ K) in CO_2 molecule with C−O bond length $l = 0.116$ nm were taken from the TraPPE force field developed by Potoff and Siepmann.[13] Partial point charges centered at each LJ site ($q_O = -0.35e$ and $q_C = 0.70e$) approximately represent the first-order electrostatic and second-order induction interactions, and the electrostatic interactions were handled using the Ewald summation technique. The above potential models have been successfully used to model the adsorptions of methane and carbon dioxide in MOFs.[4d,14] Hydrogen was treated as a diatomic molecule modeled by a LJ core located at the center of mass of it and three partial charges with two ($q = 0.468e$) located at H atoms and one ($q = -0.936e$) at the center between two H atoms. The LJ parameters for hydrogen molecule are $\sigma_{H_2} = 0.2958$ nm and $\epsilon_{H_2}/k = 36.7$ K with hydrogen bond length of 0.074 nm.[15] These parameters have been successfully used to simulate the adsorption of hydrogen in carbon nanohorns[16] and MOFs.[3g] The interactions between various sites in the adsorbed molecules were calculated by the summation of LJ interactions and the electrostatic interactions, and all the LJ cross-interaction parameters were determined by the Lorentz−Berthelot mixing rules.

For the MOFs studied here, an atomistic representation was used to model both of them. Since the all-atom OPLS (OPLS-AA) force field[17] can distinguish the types of atoms of the MOF materials in more detail and has been successfully used to model the adsorption isotherms of argon in MOFs by Vishnyakov et al.[18] and hydrogen in MOFs in our previous work,[3f,g] it was also adopted here as the force field to calculate the interactions between the adsorbate molecules and the atoms in the framework of the MOF materials.

2.3. Simulation Method. *GCMC Simulation.* GCMC simulations were employed to calculate the adsorption of pure components and their mixtures in MOF-5 and Cu-BTC. Details on the method are given elsewhere.[19] The number of the unit cells of MOFs adopted in the simulation cell varied from $4 \times 4 \times 4$ to $2 \times 2 \times 2$ so that enough molecules are accommodated to guarantee the simulation accuracy. A cutoff radius of 13 Å was applied to the LJ interactions, and the long-range electrostatic interactions were handled using the Ewald summation technique. Periodic boundary conditions were applied in all three dimensions. For each state point, the GCMC simulation consisted of 1.5×10^7 steps to guarantee equilibration followed by 1.5×10^7 steps to sample the desired thermodynamic properties. Since the adsorbent was assumed to be a rigid structure, the potential energies between an adsorbate and the adsorbent were initially tabulated on a series of three-dimensional grid points with grid spacing 0.15 Å. During the simulations, the potential energy at any position in the adsorbent was determined by interpolation.[3c,4d] It has been shown that interpolation with such grid spacing greatly increases the computational efficiency over the direct pairwise summation of adsorbate−adsorbent interaction and the accuracy of the potential energy was preserved less than 0.4%.[20] To estimate the statistical uncertainty, the production phase of each state point was divided into 10 blocks and the standard deviation of the block average was calculated. The uncertainties on the final results, including the ensemble averages of the number of adsorbate molecules in the simulation cell and the total potential energy, were estimated to be within ±2%.

Calculations for Chemical Potentials. The chemical potentials needed in the GCMC simulations were calculated from *NPT* ensemble Monte Carlo simulation using the test-particle insertion method.[21] There are no less than 512 molecules in simulation systems. In *NPT*-MC simulations, 4×10^6 configurations were generated for a state point. The first 2×10^6 configurations were discarded, and then five insertion attempts of molecules were conducted in each step. The calculated energy changes were used for the calculations of the chemical potentials.

TABLE 1: Atomic Partial Charges in the Clusters of MOF-5 and Cu-BTC Based on DFT/B3LYP Level (Unit of e)

atom name	MOF-5	Cu-BTC	atom name	MOF-5	Cu-BTC
O1C	−1.846		C1	0.667	0.778
Zn	1.501		C2	0.072	−0.092
Cu		1.098	C3	−0.132	−0.014
O1	−0.724	−0.665	H	0.140	0.109

3. Results and Discussion

3.1. Atomic Partial Charge Calculations. In our simulations, the atomic partial charges of MOF-5 and Cu-BTC are required as input parameters. The model clusters of MOF-5 and Cu-BTC used for atom partial charge calculations are shown in Figure 2. All the terminations were saturated with methyl groups. As in our previous work,[3g,4d] the electrostatic charges were used as the atomic partial charges, and the ChelpG method was adopted in this work, which has been recognized as the most popular and reliable electrostatic charge calculation method.[22] On the basis of the ChelpG method, density functional theory (DFT) calculations using the unrestricted B3LYP functional were carried out to compute the atomic partial charges, and the basis set LANL2DZ was used for atoms Zn and Cu, while 6-31+G* was used for the rest of the atoms. For heavy atoms, effective core potential (ECP) is often chosen in ab inito calculations to reduce the amount of necessary computation, and LANL2DZ is a collection of double-ζ basis sets, which is one of the most common ECP basis sets for complexes involving transition metal elements.[23] This is why we selected this basis set for atoms Cu and Zn. The calculations were performed using the GAUSSIAN 03 suite of programs,[24] and the calculated results of atomic partial charges are listed in Table 1.

Obviously, the electrostatic interactions around the corners are much stronger than that around the organic linkers in MOF-5, while in Cu-BTC, there are two kinds of domains: one is the smaller tetrahedron-shaped side pockets with strong electrostatic interactions, and the other is the larger square-shaped channels with weak electrostatic interactions. The structural differences of the two MOFs may result in different separation features as well as separation capability.

3.2. Refinement of Part OPLS-AA Force Field Parameters via Pure Gas Adsorption Isotherms. Since the parameters of the OPLS-AA force field were developed in conjunction with Monte Carlo simulations by computing thermodynamic and structural properties for pure organic liquids with the standard combining rules of $\sigma_{ij} = (\sigma_i\sigma_j)^{1/2}$ and $\epsilon_{ij} = (\epsilon_i\epsilon_j)^{1/2}$, the existing parameters may not properly represent the interactions of the atoms of the solid MOF materials with the adsorbate molecules. Therefore, part of the OPLS-AA force field parameters was refined.

For MOF-5, the energy parameters of oxygen and carbon in the phenyl group of the MOF-5 framework were adjusted to give better representation of the experimental adsorption isotherms of methane,[4a] carbon dioxide,[25] and hydrogen[26] in MOF-5 at room temperature, respectively. The parameters obtained as well as those taken from the literature are listed in Table 2, and Figure 3 shows that these parameters give very good reproduction of the experimental adsorption isotherms.

TABLE 2: Potential Parameters for the Atoms in the Framework of MOF-5

		ϵ/k (K)		
atom	σ (nm)	methane	carbon dioxide	hydrogen
O	0.296[a]	79.26[b]	63.41[b]	73.98[b]
$C_{carboxyl}$	0.375[a]	52.84[a]	52.84[a]	52.84[a]
$C_{benzene}$	0.355[a]	29.95[b]	28.18[b]	35.23[a]
$H_{benzene}$	0.242[a]	15.10[a]	15.10[a]	15.10[a]
Zn	0.246[c]	62.40[c]	62.40[c]	62.40[c]

[a] Taken from the OPLS-AA force field of Jorgensen et al.[17] [b] Obtained in this work. [c] Taken from the all-atom UFF force field (they are missed in the OPLS-AA force field).

TABLE 3: Potential Parameters for the Atoms in the Framework of Cu-BTC

		ϵ/k (K)		
atom	σ (nm)	methane	carbon dioxide	hydrogen
O	0.296[a]	61.29[b]	73.98[b]	73.98[c]
$C_{carboxyl}$	0.375[a]	42.27[b]	44.91[b]	52.84[a]
$C_{benzene}$	0.355[a]	35.23[a]	35.23[a]	35.23[a]
$H_{benzene}$	0.242[a]	15.10[a]	15.10[a]	15.10[a]
Cu	0.311[d]	2.52[d]	2.52[d]	2.52[d]

[a] Taken from the OPLS-AA force field of Jorgensen et al.[17] [b] Taken from our previous work.[4d] [c] Obtained in this work. [d] Taken from the all-atom UFF force field (they are missed in the OPLS-AA force field).

As for Cu-BTC, the potential parameters for methane and carbon dioxide have been obtained in our previous work,[4d] as listed in Table 3. To better represent the adsorption isotherm of hydrogen in Cu-BTC at 298 K, the energy parameter for O was adjusted as shown in Table 3. Figure 3b demonstrates that the parameters in Table 3 enabled a good reproduction of the corresponding experimental results of hydrogen adsorption.

To understand the adsorption behaviors of gases in these two materials at a molecular level, the snapshots of the structures of MOF-5 and Cu-BTC with adsorbed gases were examined. Three snapshots for the adsorption of carbon dioxide in MOF-5 are given as an example in Figure 4, demonstrating that the mechanism of gas adsorption in MOF-5 is as follows: gas molecules first occupy the corner regions, and the organic units start adsorbing adsorbate molecules at higher pressures, followed by the filling of the inner spaces of the cavities. This behavior has been observed commonly in zeolites.[27]

As to Cu-BTC, although some snapshots for the adsorption of carbon dioxide in Cu-BTC have been examined in our

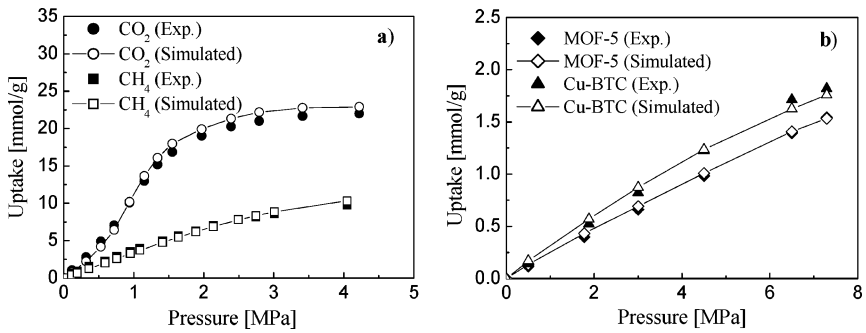

Figure 3. (a) Comparison of simulated and experimental[4a,25] adsorption isotherms of methane and carbon dioxide in MOF-5 at 298 K. (b) Comparison of simulated and experimental[26] adsorption isotherms of hydrogen in MOF-5 and Cu-BTC at 298 K.

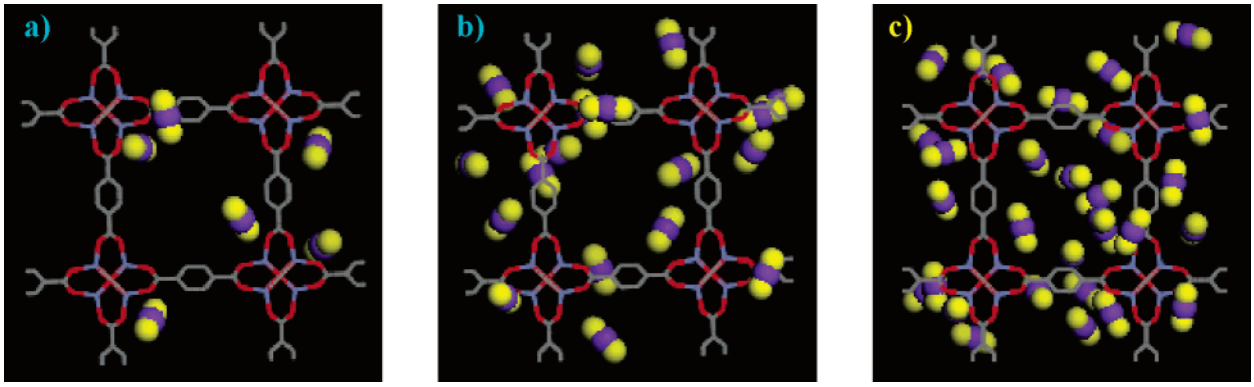

Figure 4. Snapshots of the structures of MOF-5 with adsorbed carbon dioxide at three pressures: (a) $P = 0.10$ MPa, (b) $P = 0.26$ MPa, and (c) $P = 0.70$ MPa. (MOF-5 framework is shown in line style with color: Zn, blue; O, red; C, gray; carbon dioxide: C, violet spheres, O, yellow spheres.)

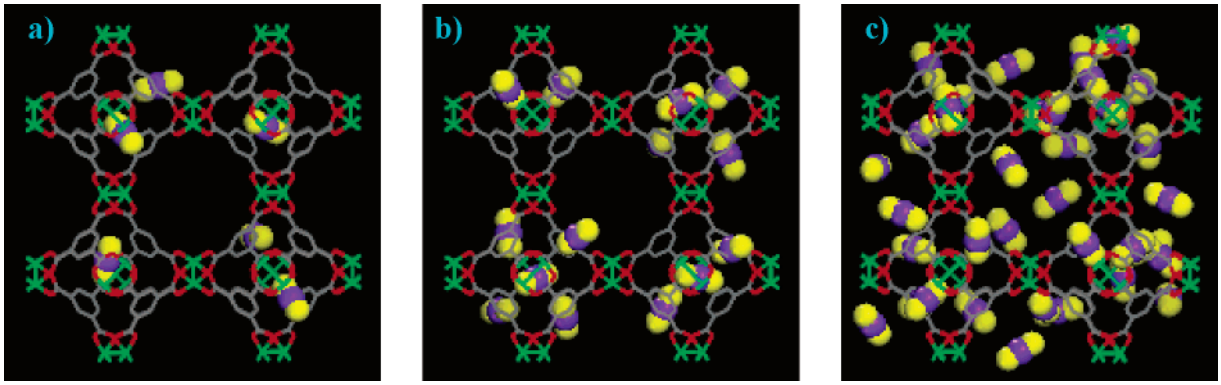

Figure 5. Snapshots of the structures of Cu-BTC with adsorbed carbon dioxide at three pressures: (a) $P = 0.012$ MPa, (b) $P = 0.028$ MPa, and (c) $P = 0.13$ MPa. (Cu-BTC framework is shown in line style with color: Cu, green; O, red; C, gray; carbon dioxide: C, violet spheres, O, yellow spheres.)

previous work,[4d] additional ones were given here to make a direct comparison with that of MOF-5, as shown in Figure 5. As can be seen from Figure 5, the sequence of gas adsorption in Cu-BTC is as follows: gas molecules first occupy the smaller tetrahedron-shaped side pockets (Figure 5a, stronger electrostatic and dispersive interaction region), followed by the saturation of the pockets (Figure 5b), and, then, they start occupying the larger square-shaped channels (weaker electrostatic and dispersive interaction region) with further increasing pressure. This behavior has also been previously observed for adsorption in zeolites such as mordenite, which has the structure with channels and side pockets.[28]

The above snapshots show that the adsorption process of gases in MOF-5 is more "homogeneous" as compared with Cu-BTC, since two kinds of pores with different structures and sizes exist in the latter. Furthermore, the sizes of the pores in Cu-BTC are smaller than that in MOF-5, leading to stronger confinement effects on those molecules accommodated.

3.3. Binary Mixtures. With these refined parameters, simulations on the adsorption of mixtures were further performed. In separation processes, a good indication of the ability for separation is the selectivity of a porous material for different components in mixtures. The selectivity for component A relative to component B is defined by $S = (x_A/x_B)(y_B/y_A)$, where x_A and x_B are the mole fractions of components A and B in the adsorbed phase, respectively, while y_A and y_B are the mole fractions of components A and B in the bulk phase, respectively.

On the other hand, it has been commonly recognized that ideal adsorbed solution theory (IAST)[29] can give good predictions of gas mixture adsorption in many zeolites,[6e,g] thus, in this work the IAST calculations were also performed to see if this is also the case for MOFs.

The simulated adsorption selectivities of methane from the equimolar binary mixture of hydrogen and methane in MOF-5 and Cu-BTC at 298 K as a function of the bulk pressure up to 5.0 MPa are shown in Figure 6a. Obviously, the adsorption selectivity behaves very differently in the two materials. For MOF-5, the selectivity of methane is nearly pressure-independent that only slightly increases with increasing pressure, while for Cu-BTC it contains two steps: a quick decrease at pressures lower than about 0.75 MPa, followed by a slow decrease with further increasing pressure. These very different behaviors can be attributed to the differences in structure. In MOF-5, as pointed out before, the crystal structure is very simple with large cubic pores; an examination of the snapshots of MOF-5 with an adsorbed hydrogen−methane mixture (Figure 7) shows that there is still much space in the pores of the material at 4.0 MPa (Figure 7b); thus, the packing effect that favors the adsorption of hydrogen is insignificant in the pressure range studied in this work. As a result, the energetic effect that favors methane adsorption is predominant, leading to a slight increase of methane selectivity with increasing pressure (loading). This observation is consistent with the previous results reported in other nanoporous materials.[6,19]

Cu-BTC, on the other hand, has two kinds of pores, and their sizes are much smaller (0.9 and 0.5 nm, respectively), leading to stronger confinement effects, and the packing effect occurred at a lower pressure (loading). As pointed out previously, both dispersive and electrostatic interactions are stronger in the side pockets than that in the channels, and thus both hydrogen and methane occupy the side pockets preferentially. The small size

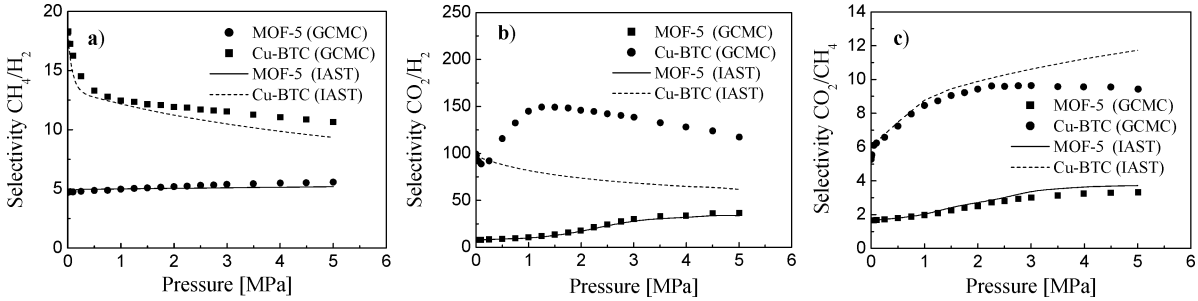

Figure 6. (a) Selectivity for methane from the equimolar mixture of hydrogen and methane in MOF-5 and Cu-BTC at 298 K. (b) Selectivity for carbon dioxide from the equimolar mixture of hydrogen and carbon dioxide in MOF-5 and Cu-BTC at 298 K. (c) Selectivity for carbon dioxide from the equimolar mixture of methane and carbon dioxide in MOF-5 and Cu-BTC at 298 K.

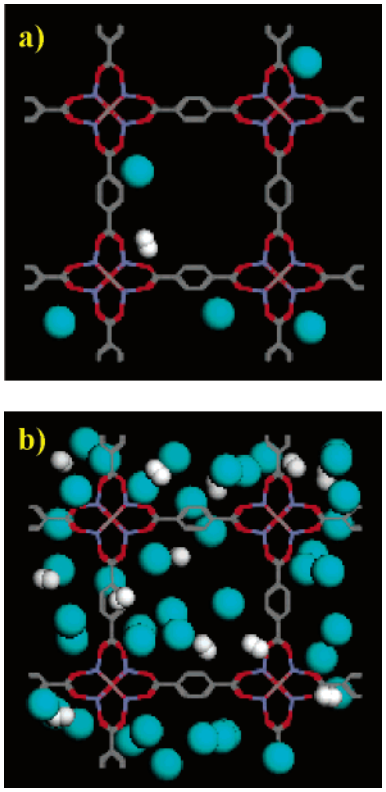

Figure 7. Snapshots of the structures of MOF-5 with adsorbed binary mixture of hydrogen and methane at two pressures: (a) $P = 0.75$ MPa and (b) $P = 4.0$ MPa. (MOF-5 framework is shown in line style with color: Zn, blue; O, red; C, gray; hydrogen, white spheres; methane: aqua spheres.)

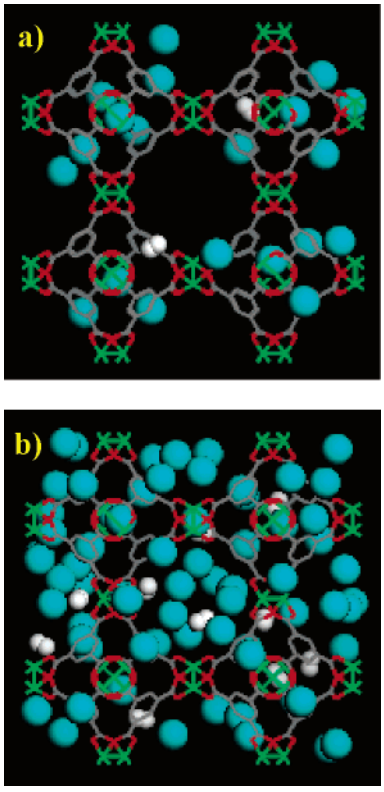

Figure 8. Snapshots of the structures of Cu-BTC with adsorbed binary mixture of hydrogen and methane at two pressures: (a) $P = 0.75$ MPa and (b) $P = 4.0$ MPa. (Cu-BTC framework is shown in line style with color: Cu, green; O, red; C, gray; hydrogen, white spheres; methane: aqua spheres.)

of the side pockets favors the packing of hydrogen, and the stronger electrostatic interactions between hydrogen and the atoms of the side pockets also enhance the adsorption of hydrogen, leading to a quick decrease of methane selectivity at low pressures. At higher pressures (higher loadings), both hydrogen and methane start occupying the channels. Although the electrostatic interactions between hydrogen and the atoms of the channels are not strong, the small size of the channels made the packing effect more significant, leading to a slight decrease of methane selectivity with further increasing pressure. The snapshots of Cu-BTC with adsorbed hydrogen−methane mixture (Figure 8) show that up to 0.75 MPa the molecules occupy mainly the side pockets (Figure 8a), while at 4.0 MPa they occupy the channels also (Figure 8b); this is consistent with our analysis as well as the above observed methane selectivity behavior.

Separation of equimolar mixture of hydrogen and methane has been performed in other porous materials; for example, at room temperature and moderate pressure, the selectivity is 8.0 in SAPO-34 membrance,[30] 2.0 in microporous SSF membrane,[31] and 13.0 in carbon nanotubes.[32] Obviously, Figure 6a indicates that Cu-BTC is a promising material for this purpose.

The adsorption selectivities of carbon dioxide from the equimolar binary mixture of hydrogen and carbon dioxide in MOF-5 and Cu-BTC at room temperature are given in Figure 6b. Again, the carbon dioxide adsorption selectivity behaves different significantly with the selectivity in Cu-BTC much larger than that in MOF-5. For MOF-5, the selectivity curve is similar to that for methane with a more evident increase with increasing pressure. The reason is the same as discussed before, and the larger increase can be attributed to the electrostatic interactions between the carbon dioxide molecules and the framework of MOF-5 as well as between the carbon dioxide molecules, these electrostatic interactions enhance more the selectivity of carbon dioxide with increasing pressure. Interestingly, in Cu-BTC, the selectivity is very sensitive to loading,

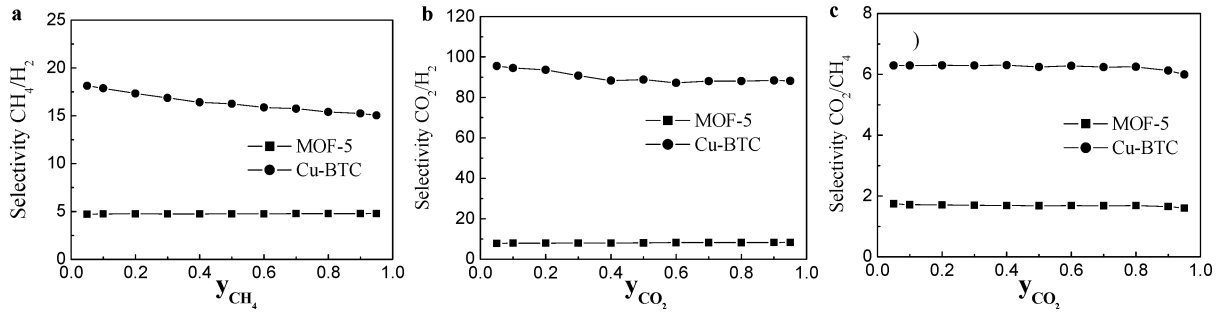

Figure 9. Composition dependency of selectivities at 0.1 MPa and 298 K: (a) CH_4/H_2 system, (b) CO_2/H_2 system, and (c) CO_2/CH_4 system.

and there exist three distinct steps in the changes of selectivity: the first step is a quick decrease of carbon dioxide selectivity at the low-pressure region, and the second one is a quick increase of its selectivity with further increasing pressure, followed by the third step of a slow decrease of carbon dioxide selectivity at high pressures. The first step is caused by the same reason as that for methane, while the second one is caused by the strong electrostatic interactions between carbon dioxide and the atoms of side pockets that enhance the adsorption of carbon dioxide in the side pockets at higher loadings, and the third step can be attributed to the fact that, at even higher pressures (loadings), the molecules occupy the channels mainly, where the electrostatic interactions are not so strong, and the packing effect starts dominating the adsorption, leading to a shape similar to that for the methane−hydrogen system.

Separation of an equimolar mixture of hydrogen and carbon dioxide has also been performed using other porous materials at room temperature and moderate pressure; for example, the selectivity is 45.0 in activated carbon[33] and 3.5 in microporous silica membrane.[34] In addition, in the low-pressure limit the selectivity is 70.65 in zeolites Na-4A for a mixture with composition CO_2:H_2 = 98.6:1.4.[8d] Thus, Figure 6b shows that Cu-BTC is a very good material for separation of hydrogen from the mixture of hydrogen and carbon dioxide.

Figure 6c shows the selectivities for carbon dioxide from the equimolar binary mixture of methane and carbon dioxide in the two materials. For MOF-5, similar behavior to that of the hydrogen−carbon dioxide mixture was observed due to the same reason, while for Cu-BTC a completely different behavior from the hydrogen−methane system was observed, which is also different from that of the hydrogen−carbon dioxide system. In this case, the selectivity of carbon dioxide shows a two-step change: a quick increase with increasing pressure at the low-pressure region, followed by a nearly independent of pressure (loading) step at high pressures (high loadings). This behavior can be explained microscopically as follows: since the dynamic sizes of carbon dioxide and methane are comparative, the packing effect is nearly identical for both gases, and the energetic effects become the predominant influencing factor in the whole pressure range. At low pressures, both gases are preferentially adsorbed in the side pockets, and the strong electrostatic interactions in the pockets enhance the adsorption of carbon dioxide greatly, leading to a quick increase on carbon dioxide selectivity with increasing pressure; at higher pressures, both gases are adsorbed in the channels, and the electrostatic interactions between the carbon dioxide molecules and the framework of Cu-BTC are weak there, leading to nearly loading-independent carbon dioxide selectivity behavior with further increasing pressure (loading).

The calculated adsorption selectivities with IAST are also shown in Figure 6. Obviously, for MOF-5 it gives good agreement with the GCMC simulations for all the systems

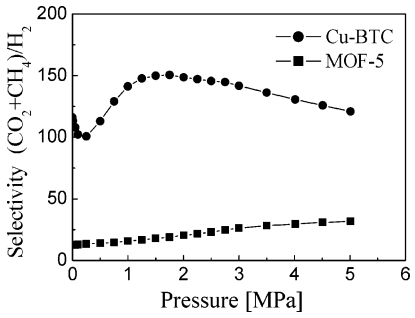

Figure 10. Pressure dependency of selectivities for (methane + carbon dioxide) from the equimolar mixture of hydrogen, methane, and carbon dioxide in MOF-5 and Cu-BTC at 298 K.

considered, while for Cu-BTC, except for CO_2/H_2, it agrees well with the GCMC simulations at low pressures. MOF-5 has a simple cubic structure; this may explain the small discrepancy between the GCMC simulations and the IAST predictions. Cu-BTC, on the other hand, has a channel/pocket complex structure with different pore sizes, leading to larger discrepancy between the GCMC simulations and the IAST predictions. The discrepancy is more significant for the CO_2/H_2 mixture since the two constituents are much different in both size and chemistry. On the basis of the above results, it seems the applicability of IAST for predicting gas mixture adsorption in MOFs is system-dependent, and fairly good results may be obtained in some cases.

For practical applications, it is useful to know how the adsorption selectivities vary with gas mixture composition; thus, additional simulations were conducted at 298 K and 0.1 MPa to make this clear. Although a useful transition matrix Monte Carlo (TMMC) method has been developed by Chen and Sholl recently that can obtain the binary isotherm for arbitrary compositions and pressures,[35] in this work we simply performed the simulations at several other compositions, and the results are shown in Figure 9. As expected, the selectivities do not strongly depend on gas mixture composition.

The simulations above show that both the pore size and the geometry of the material influence significantly the selectivity behavior of a certain gas mixture, the electrostatic interactions can enhance largely the separation efficiency for a mixture containing components with different chemistries, and selectivity steps can occur in complex MOF materials, leading to a wealth of selectivity behaviors.

3.4. Ternary Mixture. Since the purpose of purification of synthetic gas is to remove carbon dioxide and methane from the mixture mainly composed of hydrogen, carbon dioxide, and methane, it is desirable to perform simulations on the ternary mixture directly. For this purpose an equimolar ternary mixture was adopted, and the overall selectivity of carbon dioxide and methane from the ternary mixture is shown in Figure 10. The curves are similar to those for the corresponding binary mixtures

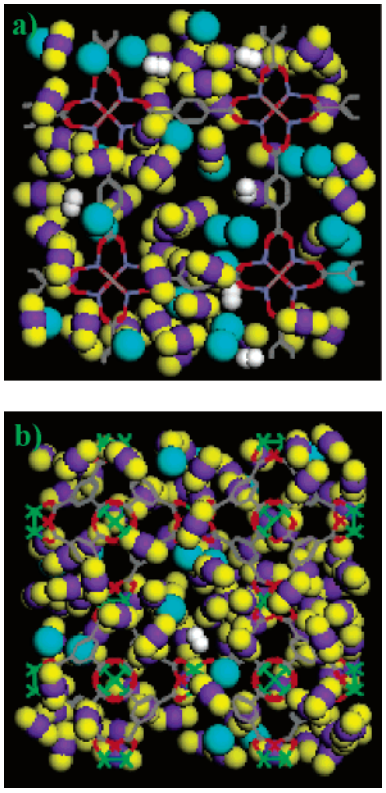

Figure 11. Snapshots of the structures of (a) MOF-5 and (b) Cu-BTC with adsorbed ternary mixture of hydrogen, methane, and carbon dioxide at $P = 3.0$ MPa. (MOF-5 and Cu-BTC frameworks are both shown in line style with color: Zn, blue; Cu, green; O, red; C, gray; hydrogen, white spheres; methane, aqua spheres; carbon dioxide, violet spheres; O, yellow spheres.)

of hydrogen and carbon due to the same mechanisms. From Figure 10, it is clear that the purification efficiency of Cu-BTC is much better than MOF-5, and the best separation efficiency for Cu-BTC at room temperature is obtained around 1.5 MPa, a condition that can be accepted practically.

The above simulations show that separation of H_2 from the mixture of $CH_4/CO_2/H_2$ using Cu-BTC should be an equilibrium-based process with high selectivities. In this case, the diffusion rates are not very important as long as diffusion is not so slow to limit charging or discharging times. The molecular dynamics simulations of Skoulidas and Sholl demonstrate that diffusivities in MOFs are similar to those in zeolites, suggesting that MOFs can meet this requirement.[3c]

To understand the structure of the materials with adsorbed ternary mixture at a molecular level, the snapshots for the two materials at $P = 3.0$ MPa are shown in Figure 11. For MOF-5, carbon dioxide molecules aggregate around the corners mainly, while the other two gases distribute in the pores mainly; as to Cu-BTC, carbon dioxide molecules occupy nearly all the side pockets, with the hydrogen and methane molecules sitting mainly in the channels. In addition, the ratios of the three gases are quite different in the two materials, leading to direct evidence that the separation efficiency of Cu-BTC is much better than MOF-5.

4. Conclusions

This work shows that both the geometry and pore size affect the separation characteristics of MOFs largely. A simple structure like MOF-5 leads to simple selectivity behaviors, while a complex structure like the channel/pocket structure of Cu-BTC can result in complex selectivity behaviors with different selectivity steps. This work also shows that electrostatic interactions can enhance greatly the separation efficiency of MOFs for gas mixtures in which the components are much different in chemistry. This work not only reveals some separation characteristics of MOFs but also elucidates the underlying mechanisms at a molecular level, providing useful microscopic information toward a complete understanding of the separation characteristics of MOFs that can lead to general design strategies for synthesizing new MOFs with tailored properties.

Acknowledgment. The financial supports of the NSFC (Grant 20476003) and the Specialized Research Fund for the Doctoral Program of Higher Education of China (Contract 20040010002) are greatly appreciated.

References and Notes

(1) (a) Pan, L.; Adams, K. M.; Hernandez, H. E.; Wang, X.; Zheng, C.; Hattori, Y.; Kaneko, K. *J. Am. Chem. Soc.* **2003**, *125*, 3062. (b) Snurr, R. Q.; Hupp, J. T.; Nguyen, S. T. *AIChE J.* **2004**, *50*, 1090. (c) Ohmori, O.; Kawano, M.; Fujita, M. *Angew. Chem., Int. Ed.* **2005**, *44*, 1962. (d) Fletcher, A. J.; Cussen, E. J.; Bradshaw, D.; Rosseinsky, M. J.; Thomas, K. M. *J. Am. Chem. Soc.* **2004**, *126*, 9750. (e) Dybtsev, D. N.; Chun, H. C.; Yoon, S. H.; Kim, D.; Kim, K. *J. Am. Chem. Soc.* **2004**, *126*, 32. (f) Schlichte, K.; Kratzke, T.; Kaskel, S. *Microporous Mesoporous Mater.* **2004**, *73*, 81. (g) Rowsell, J. L. C.; Yaghi, O. M. *Angew. Chem., Int. Ed.* **2005**, *44*, 4670.

(2) (a) Rosi, N. L.; Eckert, J.; Eddaoudi, M.; Vodak, D. T.; Kim, J.; O'Keeffe, M.; Yaghi, O. M. *Science* **2003**, *300*, 1127. (b) Kubota, Y.; Takata, M.; Matsuda, R.; Kitaura, R.; Kitagawa, S.; Kato, K.; Sakata, M.; Kobayashi, T. C. *Angew. Chem., Int. Ed.* **2005**, *44*, 920. (c) Kesanli, B.; Cui, Y.; Smith, M. R.; Bittner, E. W.; Bockrath, B. C.; Lin, W. *Angew. Chem., Int. Ed.* **2005**, *44*, 72. (d) Dinca, M.; Long, J. R. *J. Am. Chem. Soc.* **2005**, *127*, 9376. (e) Li, Y.; Yang, R. J. *Am. Chem. Soc.* **2006**, *128*, 726.

(3) (a) Sagara, T.; Klassen, J.; Ortony, J.; Ganz, E. *J. Chem. Phys.* **2005**, *123*, 014701. (b) Yildirim, T.; Hartman, M. R. *Phys. Rev. Lett.* **2005**, *95*, 215504. (c) Skoulidas, A. I.; Sholl, D. *J. Phys. Chem. B* **2005**, *109*, 15760. (d) Garberoglio, G.; Skoulidas, A. I.; Johnson, J. K. *J. Phys. Chem. B* **2005**, *109*, 13094. (e) Bordiga, S.; Vitillo, J. G.; Ricchiardi, G.; Regli, L.; Cocina, D.; Zecchina, A.; Arstad, B.; Bjørgen, M.; Hafizovic, J.; Lillerud, K. P. *J. Phys. Chem. B* **2005**, *109*, 18237. (f) Yang, Q.; Zhong, C. *J. Phys. Chem. B* **2005**, *109*, 11862. (g) Yang, Q.; Zhong, C. *J. Phys. Chem. B* **2006**, *110*, 655.

(4) (a) Düren, T.; Snurr, R. Q. *J. Phys. Chem. B* **2004**, *108*, 15703. (b) Jiang, J. W.; Sandler, S. I. *Langmuir* **2006**, *22*, 5702. (c) Pan, L.; Olson, D. H.; Ciemnolonski, L. R.; Heddy, R.; Li, J. *Angew. Chem., Int. Ed.* **2006**, *45*, 616. (d) Yang, Q.; Zhong, C. *ChemPhysChem.* **2006**, *7*, 1417.

(5) (a) Chen, B.; Liang, C.; Yang, J.; Contreras, D. S.; Clancy, Y. L.; Lobkovsky, E. B.; Yaghi, O. M.; Dai, S. *Angew. Chem., Int. Ed.* **2006**, *45*, 1390. (b) Mueller, U.; Schubert, M.; Teich, F.; Puetter, H.; Schierle-Arndt, K.; Pastré, J. *J. Mater. Chem.* **2006**, *16*, 626.

(6) (a) Krishna, R.; Smit, B.; Calero, S. *Chem. Soc. Rev.* **2003**, *31*, 185. (b) Meyer, K. M. A.; Chempath, S.; Denayer, J. F. M.; Martens, J. A.; Snurr, R. Q.; Baron, G. V. *J. Phys. Chem. B* **2003**, *107*, 10760. (c) Skoulidas, A. I.; Bowen, T. C.; Doelling, C. M.; Falconer, J. L.; Noble, R. D.; Sholl, D. S. *J. Membr. Sci.* **2003**, *227*, 123. (d) Yu, M.; Falconer, J. L.; Noble, R. D. *Langmuir* **2005**, *21*, 7390. (e) Challa, S. R.; Sholl, D. S.; Johnson, J. K. *J. Chem. Phys.* **2002**, *116*, 814. (f) Do, D. D. *Multicomponent adsorption equilibria: Adsorption analysis, equilibria, and Kinetics*; Imperial College Press: London, U.K., 2000. (g) Goj, A.; Sholl, D. S.; Akten, E. D.; Kohen, D. *J. Phys. Chem.* **2002**, *106*, 8367.

(7) Mitchell, M. C.; Gallo, M.; Nenoff, T. M. *J. Chem. Phys.* **2004**, *121*, 1910.

(8) (a) Koh, C. A.; Montanari, T.; Nooney, R. I.; Tahir, S. F.; Westacott, R. E. *Langmuir* **1999**, *15*, 6043. (b) Heuchel, M.; Davies, G. M.; Buss, E.; Seaton, N. A. *Langmuir* **1999**, *15*, 8695. (c) Nicholson, D.; Gubbins, K. E. *J. Chem. Phys.* **1996**, *104*, 8126. (d) Akten, E. D.; Siriwardane, R. Sholl, D. S. *Energy Fuels* **2003**, *17*, 977.

(9) Eddaoudi, M.; Kim, J.; Rosi, N.; Vodak, D.; Kim, J.; O'Keeffe, M.; Yaghi, O. M. *Science* **2002**, *295*, 469.

(10) Chui, S. S.-Y.; Lo, S. M.-F.; Charmant, J. P. H.; Orpen, A. G.; Williams, I. D. *Science* **1999**, *283*, 1148.

(11) Accelrys, Inc. *Materials Studio*, 3.0 V.; Accelrys Inc: San Diego, CA, 2003.

(12) Martin, M. G.; Siepmann, J. I. *J. Phys. Chem. B* **1998**, *102*, 2569.

(13) Potoff, J. J.; Siepmann, J. I. *AIChE J.* **2001**, *47*, 1676.

(14) Düren, T.; Sarkisov, L.; Yaghi, O. M.; Snurr, R. Q. *Langmuir* **2004**, *20*, 2683.

(15) Marx, D.; Nielaba, P. *Phys. Rev. A* **1994**, *45*, 8968.
(16) Tanaka, H.; Kanoh, H.; Yudasaka, M.; Iijima, S.; Kaneko, K. *J. Am. Chem. Soc.* **2005**, *127*, 7511.
(17) Jorgensen, W. L.; Maxwell, D. S.; Tirado-Rives, J. *J. Am. Chem. Soc.* **1996**, *118*, 11225.
(18) Vishnyakov, A.; Ravikovitch, P. I.; Neimark, A. V.; Bülow, M.; Wang, Q. M. *Nano Lett.* **2003**, *3*, 713.
(19) (a) Keffer, D.; Davis, H. T.; McCormick, A. V. *J. Phys. Chem.* **1996**, *100*, 638. (b) Adhangale, P.; Keffer, D. *Langmuir* **2002**, *18*, 10455.
(20) Smit, B.; Siepmann, J. I. *J. Phys. Chem.* **1994**, *98*, 8442.
(21) Shing, K. S.; Chung, S. T. *J. Phys. Chem.* **1987**, *91*, 1674.
(22) (a) Heinz, H.; Suter, U. W. *J. Phys. Chem. B* **2004**, *108*, 18341. (b) Maciel, G. S.; Garcia, E. *Chem. Phys. Lett.* **2005**, *409*, 29.
(23) (a) Foguet-Albiol, D.; O'Brien, T. A.; Wernsdorfer, W.; Moulton, B.; Zaworotko, M. J.; Abbound, K. A.; Christou, G. *Angew. Chem., Int. Ed.* **2005**, *44*, 897. (b) Davidson, E. R.; Clark, A. E. *J. Phys. Chem. A* **2002**, *106*, 7456.
(24) Frisch, M. J.; Trucks, G. W.; Schlegel, H. B.; et al. *GAUSSIAN 03*, Rev. B.1; Gaussian, Inc.: Pittsburgh, PA, 2003.
(25) Millward, A. R.; Yaghi, O. M. *J. Am. Chem. Soc.* **2005**, *127*, 17998.
(26) Panella, B.; Hirscher, M.; Pütter, H.; Müller, U. *Adv. Funct. Mater.* **2006**, *16*, 520.
(27) Van Tassel, P. R.; Davis, H. T.; McCormick, A. V. *Mol. Phys.* **1991**, *73*, 1107.
(28) Nivarthi, S. S.; Van Tassel, P. R.; Davis, H. T.; McCormick, A. V. *J. Chem. Phys.* **1995**, *103*, 3029.
(29) Myers, A. L.; Prausnitz, J. M. *AIChE J.* **1965**, *11*, 121.
(30) Poshysta, J. C.; Tuan, V. A.; Pape, E. A.; Noble, R. D.; Falconer, J. L. *AIChE J.* **2000**, *46*, 779.
(31) Vieira-Linhares, A. M.; Seaton, N. A. *Chem. Eng. Sci.* **2003**, *58*, 4129.
(32) Chen, H. B.; Sholl, D. S. *J. Membr. Sci.* **2006**, *269*, 152.
(33) Cao, D. P.; Wu, J. Z. *Carbon* **2005**, *43*, 1364.
(34) Richard, V.; Favre, E.; Tondur, D.; Nijmeijer, A. *Chem. Eng. J.* **2001**, *84*, 593.
(35) Chen, H. B.; Sholl, D. S. *Langmuir* **2006**, *22*, 709.